

Effects of Prandtl number in two-dimensional turbulent convection

Jian-Chao He(何建超), Ming-Wei Fang(方明卫), Zhen-Yuan Gao(高振源), Shi-Di Huang(黄仕迪), and Yun Bao(包芸)

Citation: Chin. Phys. B, 2021, 30 (**9**): 094701. DOI: 10.1088/1674-1056/ac0781
Journal homepage: http://cpb.iphy.ac.cn; http://iopscience.iop.org/cpb

What follows is a list of articles you may be interested in

Numerical study of heat-transfer in two-and quasi-two-dimensional Rayleigh-Bénard convection

Zhen-Yuan Gao(高振源), Jia-Hui Luo(罗嘉辉), Yun Bao(包芸)
Chin. Phys. B, 2018, 27 (**10**): 104702. DOI: 10.1088/1674-1056/27/10/104702

Boundary layer flow and heat transfer of a Casson fluid past a symmetric porous wedge with surface heat flux

Swati Mukhopadhyay, Iswar Chandra Mandal
Chin. Phys. B, 2014, 23 (**4**): 044702. DOI: 10.1088/1674-1056/23/4/044702

Heat transfer for boundary layers with cross flow

Krishnendu Bhattacharyya, Ioan Pop
Chin. Phys. B, 2014, 23 (**2**): 024701. DOI: 10.1088/1674-1056/23/2/024701

Variable fluid properties and variable heat flux effects on the flow and heat transfer in a non-Newtonian Maxwell fluid over an unsteady stretching sheet with slip velocity

Ahmed M. Megahed
Chin. Phys. B, 2013, 22 (**9**): 094701. DOI: 10.1088/1674-1056/22/9/094701

Influence of polymer additives on turbulent energy cascading in forced homogeneous isotropic turbulence studied by direct numerical simulations

Li Feng-Chen, Cai Wei-Hua, Zhang Hong-Na, Wang Yue
Chin. Phys. B, 2012, 21 (**11**): 114701. DOI: 10.1088/1674-1056/21/11/114701

Effects of Prandtl number in two-dimensional turbulent convection*

Jian-Chao He(何建超)[1], Ming-Wei Fang(方明卫)[1], Zhen-Yuan Gao(高振源)[2,3], Shi-Di Huang(黄仕迪)[2,3], and Yun Bao(包芸)[1,†]

[1] School of Aeronautics and Astronautics, Sun Yat-sen University, Guangzhou 510275, China
[2] Center for Complex Flows and Soft Matter Research and Department of Mechanics and Aerospace Engineering, Southern University of Science and Technology, Shenzhen 518055, China
[3] Guangdong Provincial Key Laboratory of Turbulence Research and Applications, Southern University of Science and Technology, Shenzhen 518055, China

(Received 21 March 2021; revised manuscript received 7 May 2021; accepted manuscript online 3 June 2021)

We report a numerical study of the Prandtl-number (Pr) effects in two-dimensional turbulent Rayleigh–Bénard convection. The simulations were conducted in a square box over the Pr range from 0.25 to 100 and over the Rayleigh number (Ra) range from 10^7 to 10^{10}. We find that both the strength and the stability of the large-scale flow decrease with the increasing of Pr, and the flow pattern becomes plume-dominated at high Pr. The evolution in flow pattern is quantified by the Reynolds number (Re), with the Ra and the Pr scaling exponents varying from 0.54 to 0.67 and -0.87 to -0.93, respectively. It is further found that the non-dimensional heat flux at small Ra diverges strongly for different Pr, but their difference becomes marginal as Ra increases. For the thermal boundary layer, the spatially averaged thicknesses for all the Pr numbers can be described by $\delta_\theta \sim Ra^{-0.30}$ approximately, but the local values vary a lot for different Pr, which become more uniform with Pr increasing.

Keywords: turbulent convection, Prandtl number, direct numerical simulations (DNS)

PACS: 47.27.te **DOI:** 10.1088/1674-1056/ac0781

1. Introduction

Turbulent convection exists widely in nature and engineering applications. Rayleigh–Bénard (RB) convection, a fluid layer heated from below and cooled from above, has been a paradigmatic model to study the convection phenomena.[1–3] For RB system in a particular geometry, its dynamics is mainly controlled by two dimensionless parameters, namely, the Rayleigh number $Ra = \alpha g \Delta T H^3/(\nu\kappa)$ and the Prandtl number $Pr = \nu/\kappa$. The Ra number characterizes the ratio of the buoyancy force to the damping force due to viscous and thermal dissipations. And the Pr number, defined by the properties of working fluid, represents the relative importance of viscous and thermal diffusions. Here, α, ν, and κ are the thermal expansion coefficient, the kinematic viscosity and the thermal diffusivity of the working fluid, respectively, ΔT is the temperature difference across the fluid layer with the height being H, and g is the gravitational acceleration.

The global responses of the turbulent RB convection that people most concern are the heat transfer efficiency and the strength of turbulent flow, which are indicated by the Nusselt number Nu and the Reynolds number Re, respectively. Over the years, how the two response parameters depend on the system's control parameters, i.e., the relations of $Nu(Ra, Pr)$ and $Re(Ra, Pr)$, is the utmost important issue in the study of the turbulent RB convection. Many theories have been proposed to address this issue[4–9] and the model developed by Grossmann and Lohse (GL)[10,11] turns out to be the most successful one so far. However, while the GL model has been widely verified regarding to the Ra dependence of Nu and Re, the Pr dependent behaviors have received less attention.[1,12]

The study on the Pr-number effect in the RB convection can be traced back to the work by Globe and Dropkin in 1959.[4] By using different kinds of working fluids, including water, silicon oils and mercury, they achieved a wide Pr range from 0.02 to 8750 with the Ra number up to 6.8×10^8. Based on the experimental data, they reported a simple relation as $Nu = 0.069 Ra^{1/3} Pr^{0.074}$, suggesting that the heat transport efficiency increases monotonically with Pr. However, it was pointed out in the GL model that there exists no pure power law for the $Nu(Ra, Pr)$ relation.[10,11] Indeed, by conducting direct numerical simulations in a flat box for $10^4 < Ra < 10^7$, Kerr and Herring[13] found that Nu obeys a $Ra^{2/7}$ power law approximately at $Pr = 7$ and 0.3, but the relation approaches to $Ra^{1/4}$ at $Pr = 0.07$. Later studies further found that the $Nu(Ra)$ scaling increases to around 0.3 as Pr increases,[14–17] which eventually becomes $1/3$ in the very large Pr regime (say, $Pr > 10^4$).[11,18] The $Nu(Pr)$ relation exists no simple exponent value either. While the $Nu(Pr)$ scaling obtained by simulations was 0.14 for $0.022 \le Pr \le 0.35$ at $Ra = 6\times10^5$,[19] its value changes to be 0.18–0.22 for $0.001 \le Pr \le 0.3$ at

*Project supported by the National Natural Science Foundation of China (Grant Nos. 11961160719, 11702128, 91752201, and 11772362), the Shenzhen Fundamental Research Program (Grant No. JCYJ20190807160413162), the Fundamental Research Funds for the Central Universities (Sun Yat-sen University under Grant No. 19lgzd15), and the Department of Science and Technology of Guangdong Province, China (Grant No. 2019B21203001).

†Corresponding author. E-mail: stsby@mail.sysu.edu.cn

© 2021 Chinese Physical Society and IOP Publishing Ltd

$Ra = 10^6$,[20] both of which are noticeably different from the value of 0.074 obtained in the experiment.[4] Moreover, as Pr is larger than ~ 3, instead of increasing monotonically, Nu becomes a decreased function of Pr, though the dependence is rather weak and even negligible.[13–24] Most of these features of the $Nu(Ra, Pr)$ relation can be captured by the GL model,[10–12] which is believed to be an indicator of the model's success.

Besides the heat transport behavior, the flow morphology and dynamics also evolve with Ra and Pr. It was revealed that the turbulent flow at low Pr number is dominated by a large scale recirculation cell, whereas thermal plumes (the elementary heat objects in the system) take over the role at high Pr number.[19,25] As a result, the Re number differs a lot for different Pr regimes. The numerical study by Verzicco *et al.*[19] showed that Re scales as $Pr^{-0.73}$ when $Pr < 0.35$, but the scaling exponent changes to -0.94 when $Pr > 0.35$. On the other hand, because direct measurement of the velocity fields is technically inaccessible for most working fluids, many approaches were proposed to measure the Re number, including the maximum velocity, the root-mean-square (rms) velocity, and the oscillation frequency of the LSC (or temperature).[17,26] It is found that the Ra and the Pr scaling exponents of Re based on different definitions change from 0.4 to 0.68 and -0.72 to -0.95, respectively. These results are so divergent that some are in agreement with the predictions of the GL model, but some are not.[27]

Note that all the studies mentioned above were made in the three-dimensional (3D) RB system, which is fundamentally different from the GL model developed from two-dimensional (2D) equations in essence. Recently, due to the discovery of heat-transport enhancement in the slim-box, turbulent convection in quasi-2D system has become one important topic in the community of RB convection (see, e.g., Refs. [28–30]). However, quasi-2D system is still fundamentally different from the true 2D case. Thanks to the growing studies of the RB convection in 2D configuration, it has been shown that the 2D RB system differs from the 3D (and quasi-2D) case in many aspects.[21,23,31,32] For example, Schmalzl *et al.*[21] found that the Nu data in 2D RB flow at $Ra = 10^6$ have no obvious Pr-dependence in the range of $0.01 \leq Pr \leq 100$, and the Re number diverges from the 3D data when Pr is smaller than unity. Huang and Zhou [31] further found that 2D RB convection exhibits a minimum Nu at $Pr = 2$–3 for $10^8 \leq Ra \leq 10^9$, which is in strong contrast to the maximum value found in the 3D case. van der Poel *et al.*[23] also observed a number of differences between 2D and 3D RB systems, despite that they share some similarities in flow pattern. However, these studies in 2D RB configuration were made at either limited Pr ranges or relative low Ra values. To have a complete understanding of turbulent RB convection in 2D geometry, it is essential to explore a much wider Ra–Pr range.

In this paper, we present a systematic study of the 2D RB convection using direct numerical simulations (DNS), with the Ra and Pr ranges as wide as three orders in the turbulent regime. We first make a detailed comparison of the flow patterns at different Pr, and then examine the Pr-number effects on the Re number, the Nu number and thermal boundary layer. These results not only enrich our understanding of the 2D turbulent convection, but also provide a useful data base for model testing and development in the future.

2. Numerical methods and parameters

The non-dimensional governing equations for RB convection under Boussinesq approximation are as follows:

$$\begin{aligned}
&\nabla\cdot u = 0,\\
&\frac{\mathrm{d}u}{\mathrm{d}t} = -\nabla P + \frac{1}{\sqrt{Ra/Pr}}\nabla^2 u + \theta\hat{z},\\
&\frac{\mathrm{d}\theta}{\mathrm{d}t} = \frac{1}{\sqrt{Ra\cdot Pr}}\nabla^2\theta,
\end{aligned}$$

where u, P, θ, and $\hat{z}$ represent, respectively, the non-dimensional velocity, pressure, temperature and the vertical unit vector with its direction opposite to gravity. We numerically solve the above equations with a high-efficient parallel direct method, which is based on a second-order finite difference scheme.[33] The simulations are made in a square box, thus the aspect ratio Γ of the system is equal to one. The boundary conditions are set as no-slip for velocity and impermeable for pressure on all the walls. The top and bottom boundaries are fixed at constant temperatures, with their values being $\theta_{\mathrm{top}} = -0.5$ and $\theta_{\mathrm{bot}} = 0.5$, respectively. The left and right sidewalls are adiabatic.

Figure 1 shows the Ra–Pr phase diagram covered in the present study, with the Ra number ranging from 10^7 to 10^{10} and the Pr number ranging from 0.25 to 100. The determination of the parameter ranges is based on two considerations. The first one is that the simulated cases should be largely in the turbulent regime, as we focus on studying turbulent convection. According to the GL model,[10] the boundary between laminar flow to turbulent convection is indicated by the solid line in Fig. 1. Second, we recently observed a new flow regime that deviates from the prediction of the GL model, which is triggered by an anomalous transition in the large-scale flow.[34] This transition is indicated by the dashed line in Fig. 1, so we did not go to low Pr numbers for larger Ra. To resolve the smallest turbulent scales and the boundary layers sufficiently, we set the meshes and time intervals for different parameters according to the criteria proposed by Gao *et al.*[32] The relative errors of Nu based on different calculating methods[36] are smaller than 1% for all the cases, indicating that our simulations are well resolved and statistically converged.

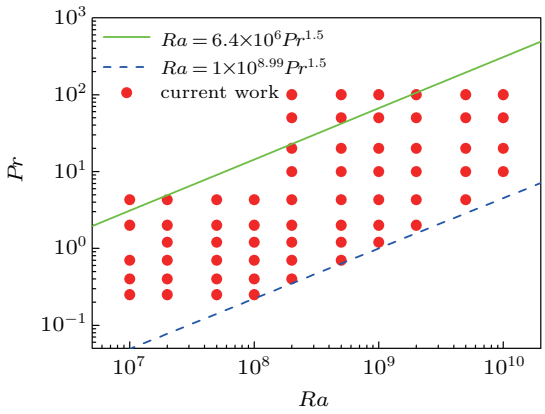


Fig. 1. The *Ra*–*Pr* Phase diagram explored in the present study. The solid line indicates the transition from laminar flow to turbulence[10] and the dashed line indicates another newly-observed transition in the large-scale flow.[34] See text for detailed explanations.

Note that irregular reversal of the large-scale flow circulating directions occurs at certain range of *Ra*–*Pr* in the present study, i.e., $Ra = 5\times10^7$–3×10^8 for $Pr = 4.3$, $Ra = 1\times10^7$–1×10^8 for $Pr = 2.0$, and $Ra = 2\times10^7$ for $Pr = 1.2$, respectively. To check whether these reversal processes would affect the *Nu* and *Re* numbers, we calculated their values when the large-scale flow circulates in either clockwise or anticlockwise direction, and found that the obtained values of *Nu* and *Re* are the same for both directions. We have also calculated *Nu* and *Re* when reversal processes are involved. It turns out that the change in *Nu* is no more than 3%, but the *Re* number decreases by 50% due to the dramatic change in flow field during flow reversal. Similar findings have been reported in some previous studies.[37–39] As we need to compare the results in a wide range of *Ra*–*Pr*, where most of the cases have no flow reversals, in the present study we calculated *Nu* and *Re* without considering the reversal processes. It is also noteworthy that the simulations were run for at least 200 (but no more than 500) free-fall time for each set of *Ra*–*Pr*. While these computation times are sufficient for calculating *Nu* and *Re*, they are far from enough for doing statistical analysis of flow reversal. A detailed study of flow reversal should be subject to future studies.

3. Results and discussion

3.1. Flow pattern

We first examine how the flow pattern in the 2D RB convection evolves with *Ra* and *Pr*. Figure 2 shows some typical snapshots of flow fields at $Ra = 2\times10^8$ for different *Pr* numbers. Note that the red and blue structures in the temperature fields [Figs. 2(a)–2(d)] represent hot and cold thermal plumes, respectively. It can be seen that, for the $Pr = 0.4$ case, the flow pattern in the system is dominant by a large-scale circulation (LSC) that expands almost the whole domain diagonally. Forced by the strong motion of the LSC, most of the thermal plumes are taken away directly after detaching from the thermal boundary layer and move along the sidewalls. The rest plumes are trapped at the remaining corners and form two counter-rotating secondary rolls. The flow pattern at $Pr = 4.3$ is qualitatively the same, except that the LSC is more elliptical and the corner rolls are a bit larger. This kind of flow pattern and the associated dynamics have been well recognized before.[36,40]

However, as *Pr* increases to 20, the LSC's motion becomes less organized and the corner rolls are less identified. On the other hand, the thermal plumes become slimmer, suggesting that they are more coherent and less dissipative.[16] When *Pr* further increases to 100, the flow pattern totally changes. Rather than dominated by a system-sized LSC, the whole domain is occupied by random motion of thermal plumes, which pass through the bulk region in a more straight way. The breakdown of the LSC at large *Pr* has been also observed in a quasi-2D RB experiment very recently,[25] but it occurs at much larger *Pr* and *Ra* numbers. It is noteworthy that this breakdown coincides with the transition from laminar flow to turbulent regime aforementioned, confirming the essential role of the LSC in turbulent RB system.[10,11]

The evolution in flow pattern is also revealed by the vertical velocity field, which is inherently linked to the movement of thermal plumes. This is evident by the distributions of the red and blue structures (indicating upward and downward moving fluid, respectively) as shown in Figs. 2(e)–2(h). It is seen that, at low *Pr* numbers, the vertical motion is mainly concentrated at the left and right sides of the system, with the velocity in the central region being marginal. As *Pr* increases, the distribution of the vertical motion becomes less concentrated and even irregular, which reflects the fact that the LSC is less stable with increasing *Pr* and disappears eventually. As a result, the flow strength reduces greatly, with the maximum vertical velocity decreasing almost one order of magnitude for the cases shown in Fig. 2. These results suggest that the effects of the *Pr* number are twofold. The first one is changing the viscous damping force as expected, which influences the flow strength directly. The second one is coupled with the first one: the change in flow strength will modify the organized pattern of flow structures, which in turn affects the flow strength further.

As the 2D RB convection at $Pr > 10$ has been rarely studied, we take the $Pr = 20$ case to discuss the influence of the *Ra* number on flow pattern. It is seen in Figs. 2(a)–2(d) that the flow patterns are quite similar for different *Ra* numbers, though the LSC and the corner rolls at $Ra = 2\times10^8$ are not well developed yet. This similarity can also be observed in the distributions of vertical velocity as shown in Figs. 3(e)–3(h). While there is no qualitative difference in the large-scale flow, the thermal plumes are found to be more fragmentary as *Ra* increases. This is supported by the small flow structures appearing in Figs. 3(f)–3(h), which could be understood with the strong fluctuation with the increasing *Ra*.

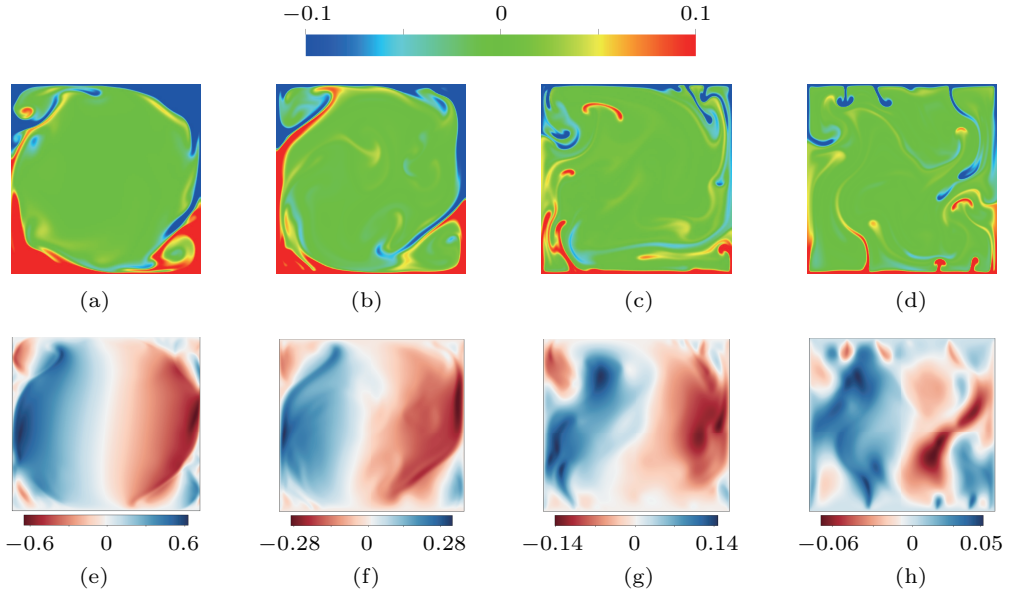


Fig. 2. Instantaneous temperature (a)–(d) and vertical velocity (e)–(f) fields at $Ra = 2 \times 10^8$ for different Pr numbers: $Pr = 0.4$ (a) and (e), $Pr = 4.3$ (b) and (f), $Pr = 20$ (c) and (g), and $Pr = 100$ (d) and (h). In order to show the flow structures more clearly, the temperature color map is set between −0.1 to 0.1. The color bars for the velocity fields are based on their own variation ranges.

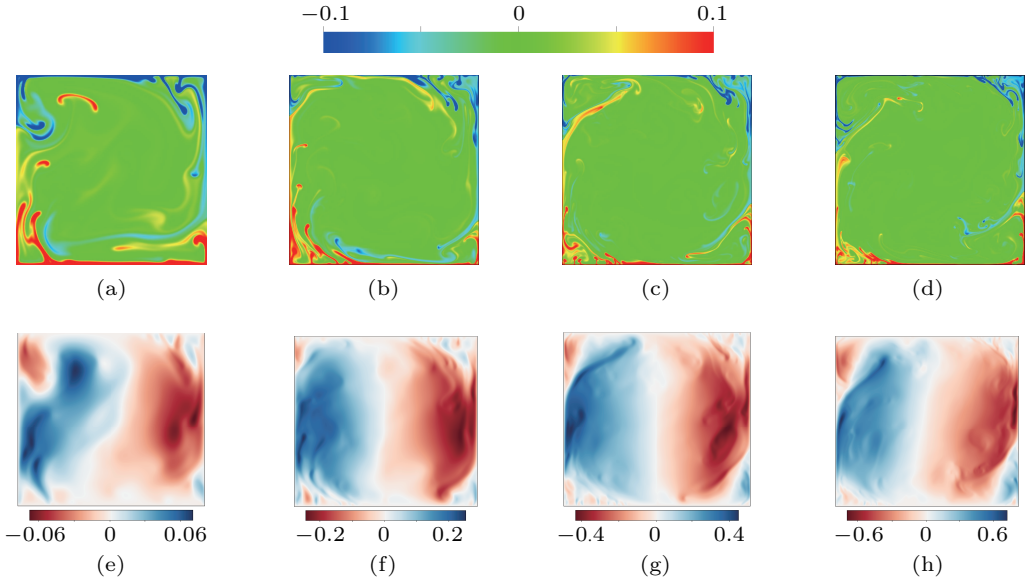


Fig. 3. Instantaneous temperature (a)–(d) and vertical velocity (e)–(f) fields at $Pr = 20$ for different Ra numbers: $Ra = 2 \times 10^8$ (a) and (e), $Ra = 2 \times 10^9$ (b) and (f), $Ra = 5 \times 10^9$ (c) and (g), and $Ra = 1 \times 10^{10}$ (d) and (h). The temperature color map is the same as that in Fig. 2. In order to distinguish the effect of Ra, the color bars for the velocity fields are based on their own velocity variation ranges, which have been re-scaled by the dimensional velocity for real fluid (silicone oil used in the experiment by Li *et al.*[25]).

3.2. Reynolds number

To quantify the above changes in flow pattern, we turn to investigate the $Re(Ra, Pr)$ relation. Because the detailed flow features differ strongly for different parameters, we use the rms velocity $U_{\rm rms} = \sqrt{\langle (u^2 + v^2) \rangle_{V,t}}$ as the characteristic flow velocity. Here, $\langle . \rangle_{V,t}$ represents an average over the whole domain and all the time after the flow reaches equilibrium. Thus, the so-defined Re number $Re = U_{\rm rms} H/\nu$ can well represent the turbulent strength of the system.

Figure 4 shows how the Re number depends on Ra and Pr. It is seen that all the data can be well described by power-law fittings, but their scaling exponents are non-universal (see Table 1). To be specific, the scaling exponent α for $Re \sim Ra^{\alpha}$ is equal to 0.54 for $Pr = 0.25$, then increases to ~ 0.60 for $Pr > 1$,[23,35,41] and finally exhibits a sudden growth to 0.67 for $Pr = 100$. This variation trend of α is consistent with a recent experimental finding in the quasi-2D RB system,[25] which was attributed to the evolution in the large-scale flow pattern.

However, all the α values in the present study are appreciably larger than previous results obtained in 3D system and the GL model's prediction (varying from 0.4 to 0.5).[1,10,11] This discrepancy is somewhat surprising, especially given that the GL model essentially is a 2D model. It could be due to

that the inverse energy cascade in 2D turbulence contributes to a stronger driven force for the large-scale flow, which has not been considered in the existing models for turbulent convection. It is worthwhile to develop a model involved inverse cascade process in the future.

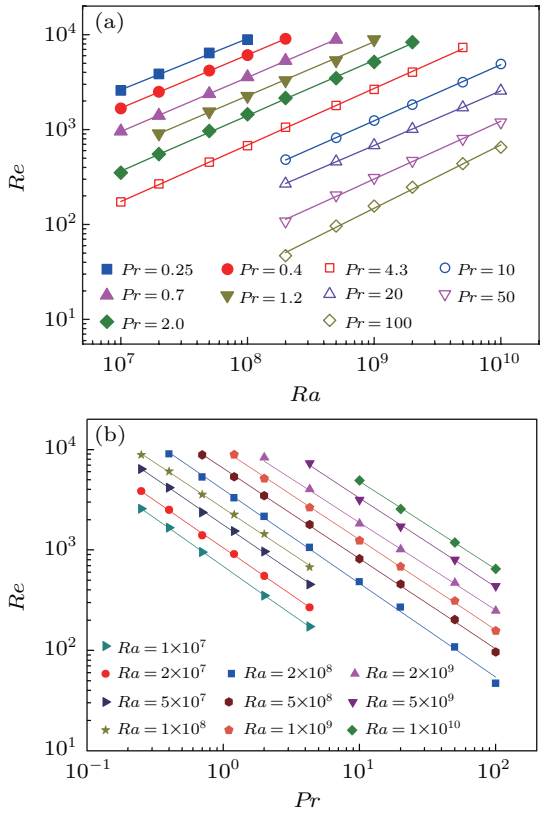


Fig. 4. Log–log plots of *Re* as a function of *Ra* (a) and *Pr* (b). The solid lines are the best power-law fits to the corresponding datasets. The fitting results are listed in Table 1.

Table 1. The power-law fitting results for $Re \sim Ra^{\alpha}$ at different *Pr* and $Re \sim Pr^{\beta}$ at different *Ra*.

Pr	α	*Ra*	β
0.25	0.54	1×10^7	−0.93
0.4	0.56	2×10^7	−0.93
0.7	0.54	5×10^7	−0.92
1.2	0.57	1×10^8	−0.93
2	0.58	2×10^8	−0.93
4.3	0.60	5×10^8	−0.90
10	0.59	1×10^9	−0.87
20	0.57	2×10^9	−0.87
50	0.61	5×10^9	−0.89
100	0.67	1×10^{10}	−0.87

The scaling exponent β of $Re \sim Pr^{\beta}$ is not a universal constant, either. Their values for different *Ra* are found to be varied from −0.93 to −0.87 (see Table 1). These negative exponents provide a quantification to Fig. 2 that how the flow strength decreases with *Pr*. When compared with the previous studies of 3D RB convection, the present *Pr*-dependences are slightly weaker than the simulation results (changing from −0.94 to −1),[14,18–21] but stronger than the experimental findings (varying from −0.76 to −0.86).[17,26] According to the GL model, the value of β for the present parameter ranges should be in between −0.67 to −0.83, which could not explain the exponents obtained in the present study. Combined with the discrepancy in the $Re \sim Ra^{\alpha}$ relation discussed above, it is highly desired to revise the GL model for the 2D RB convection.

3.3. Nusselt number

It has been shown that the heat transport efficiency in 2D RB convection has a sensitive dependence on the system's aspect ratio, which was ascribed to the change in flow structures.[42,43] Since we observe a pronounced effect of *Pr* on the flow pattern, it is interesting to check the associated heat transport properties. Figure 5 shows the *Ra* and *Pr* dependences of the Nusselt number *Nu*, which is calculated by the formula below:[35]

$$Nu = \sqrt{Ra \cdot Pr}\langle u_z \theta \rangle_{V,t} - \langle \partial_z \theta \rangle_{V,t}.$$

In order to distinguish the datasets for different *Pr*, we normalized *Nu* with $Ra^{0.3}$ by convention in Fig. 5(a). Note that we have checked the error for the *Nu* data, and found that all the errors are smaller than 1% in our simulated cases. Therefore, an error bar of 1% is shown in Fig. 5(a) for reference. It is seen that the compensated *Nu* can be roughly divided into two groups. For *Pr* smaller than 4.3, the data first grow remarkably as *Ra* increases and then saturate at a plateau after $Ra = 2\times10^8$. However, for higher *Pr* cases, the results decrease slightly with a similar trend with increasing *Ra*. These behaviors suggest that the *Ra*-dependent exponent are larger than 0.3 for low *Pr* cases but smaller than 0.3 for high *Pr* cases. It is further found that, when *Ra* is small, the compensated *Nu* diverges strongly for different *Pr*. As *Ra* increases, their differences become smaller and finally coincide with each other. As previous studies were conducted in limited *Ra* and *Pr* ranges,[21,23,31,32] these complex heat transport behaviors have not been observed before. Thus, our data provide a more complete picture of the heat transport in the 2D RB convection.

A great success of the GL model was the good agreement with the experimental *Nu* data in 3D RB system over a wide *Pr* range.[12,15] Recently, it is further found that the GL model's prediction can also capture the *Nu* data in quasi-2D system, only differing by a constant factor.[25] Now we check how the *Nu* data in 2D system compare to the GL model. It is seen from Fig. 5(b) that, once the GL predicting curves are shifted down by certain constant factors, most of the data can be described by the GL model as well. The shifted factors range from 0.72 to 0.85, which are smaller than those values (0.93–0.98) in the quasi-2D case. This suggests that the 2D RB convection has a lower heat transfer efficiency than both quasi-2D and 3D systems. In addition, combined the present

results with previous studies,[17,21,23] we can further conclude that heat transfer in the RB convection is insensitive to Pr when Pr is greater than 10, regardless of the geometries of the system.

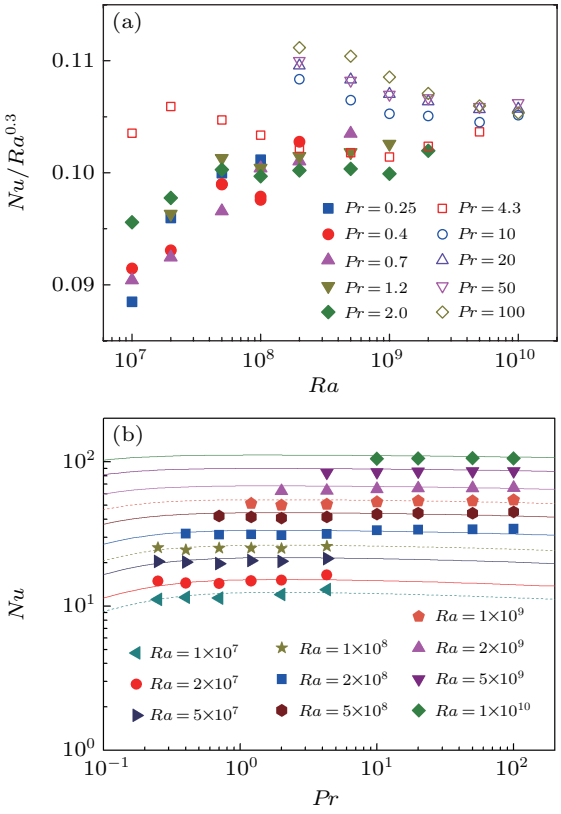


Fig. 5. (a) Compensated Nu with $Ra^{0.3}$ as a function of Ra and (b) Nu as a function of Pr. The lines in panel (b) are the predictions of the updated GL model[12] multiplied by 0.72, 0.73, 0.80, 0.80, 0.83, 0.84, 0.84, 0.85, 0.85, and 0.85 from lowest to highest Ra, respectively.

3.4. Thermal boundary layer

The thermal boundary layer is not only closely related to the heat transfer efficiency, but can also be modified by the flow dynamics. In this subsection, we study the Pr effect on the thickness of thermal boundary layer δ_θ, which is determined by the widely used "slope method" in the study of turbulent RB convection.[1] It is obvious in Fig. 6(a) that, with increasing Ra, the spatially-averaged thermal boundary layer gets thinner and the data for different Pr become undistinguished for each other at higher Ra, which are consistent with the Nu results. If a power law fit is attempted to all the data shown in Fig. 6(a), we yield a power law as $\delta_\theta \sim Ra^{-0.30}$, in agreement with previous studies at medium Pr.[21,23,32] Although the mean values of thermal boundary layer thickness for different Pr are not much different, the local boundary layer values differ a lot. It is seen in Fig. 6(b) that the spatial variation in the boundary layer thickness is stronger for lower Pr, with the thinnest region related to the shearing of the LSC and the two peaks related to the corner rolls. As Pr increases, the thinnest boundary layer in the LSC shear region get thicker, manifesting the fact that the shearing of LSC attenuates; and the two peaks gradually vanishes, corresponding to the weakening of the corner rolls. As the LSC breaks down at $Pr = 100$, the thermal boundary layer eventually becomes quite uniform along the conducting boundaries. These results well reflect the changes in the flow pattern as shown in Fig. 2.

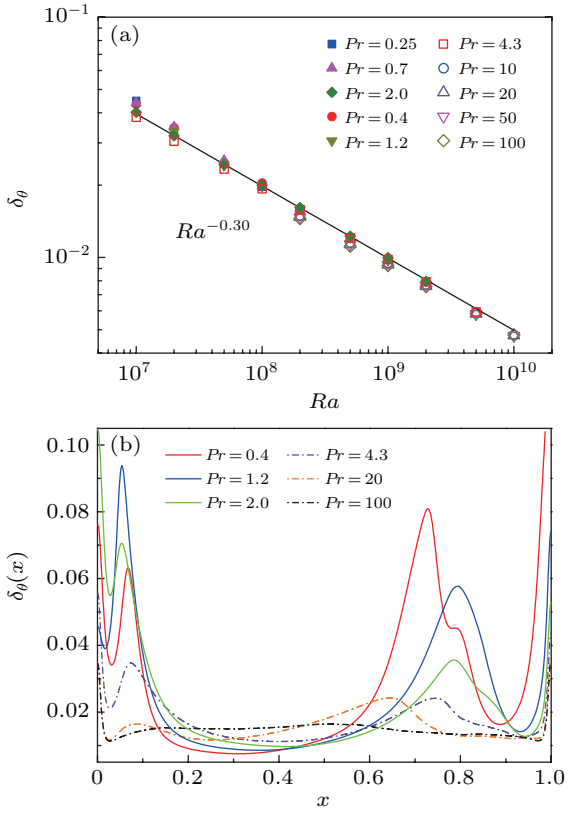


Fig. 6. (a) Log–log plots of δ_θ as a function of Ra. The solid line is the best power-law fit of all data therein. (b) The thermal boundary layer thickness $\delta_\theta(x)$ along the bottom boundary at $Ra = 2\times10^8$ for different Pr numbers.

4. Conclusion and perspectives

In this paper, we numerically simulated the 2D RB convection over unprecedentedly wide parameter ranges, i.e., $10^7 \le Ra \le 10^{10}$ and $0.25 \le Pr \le 100$. The flow pattern, the Re number, the Nu number and the thermal boundary layer are investigated in detail, with a focus on the Pr effects. The major findings are summarized as below.

(i) The Pr number has a strong influence on both the flow pattern and the flow strength. As Pr increases, both the LSC and the corner rolls become weaker and disappear eventually. The flow pattern becomes dominated by random motion of thermal plumes at high Pr number.

(ii) There is no a simple power law for the $Re(Ra, Pr)$ relation. It is found that the Ra and the Pr scaling exponents of Re change from 0.54 to 0.67 and -0.87 to -0.93, respectively, which are inconsistent with the predictions of the GL model. It is worthwhile to revise the GL model to coincide with these discrepancies.

(iii) The Nu data for different Pr diverge strongly at small Ra, but their difference becomes marginal as Ra increases. All the Nu data can be well captured by the GL model's predictions after shifting certain constant factors. Our results also suggest that the heat transfer efficiency in the 2D RB convection is smaller than those in the quasi-2D and 3D systems.

(iv) The thermal boundary layer thickness δ_θ can be described by a simple power law as $\delta_\theta \sim Ra^{-0.30}$. Due to the influences from the corner rolls and the LSC, the local thermal boundary layer $\delta_\theta(x)$ varies a lot along the bottom plat at low Pr number. But this variation becomes smaller as Pr increases and $\delta_\theta(x)$ eventually gets uniform at high Pr number.

Acknowledgment

The authors would like to thank the computational sources provided by the Center for Computational Science and Engineering at Southern University of Science and Technology.

References

[1] Ahlers G, Grossmann S and Lohse D 2009 *Rev. Mod. Phys.* **81** 503
[2] Lohse D and Xia K Q 2010 *Annu. Rev. Fluid Mech.* **42** 335
[3] Xia K Q 2013 *Theor. Appl. Mech. Lett.* **3** 052001
[4] Globe S and Dropkin D 1959 *J. Heat Transfer* **81** 24
[5] Davis A H 1922 *Phil. Mag.* **43** 329
[6] Davis A H 1922 *Phil. Mag.* **44** 920
[7] Heslot F, Castaing B and Libchaber A 1987 *Phys. Rev. A* **36** 5870
[8] Castaing B, Gunaratne G, Heslot F, Kadanoff L, Libchaber A, Thomae S, Wu X Z, Zaleski S and Zanetti G 1989 *J. Fluid Mech.* **204** 1
[9] Shraiman B I and Siggia E D 1990 *Phys. Rev. A* **42** 3650
[10] Grossmann S and Lohse D 2000 *J. Fluid Mech.* **407** 27
[11] Grossmann S and Lohse D 2001 *Phys. Rev. Lett.* **86** 3316
[12] Stevens R J A M, van der Poel E P, Grossmann S and Lohse D 2013 *J.Fluid Mech.* **730** 295
[13] Kerr R M and Herring J R 2000 *J. Fluid Mech.* **419** 325
[14] Silano G, Sreenivasan K R and Verzicco R 2010 *J. Fluid Mech.* **662** 409
[15] Xia K Q, Lam S and Zhou S Q 2002 *Phys. Rev. Lett.* **88** 064501
[16] Pandey A and Verma M K 2016 *Phys. Fluids* **28** 095105
[17] Yang Y H, Zhu X, Wang B F, Liu Y L and Zhou Q 2020 *Phys. Fluids* **32** 015101
[18] Shishkina O, Emran M S, Grossmann S and Lohse D 2017 *Phys. Rev. Fluids* **2** 103502
[19] Verzicco R and Camussi R 1999 *J. Fluid Mech.* **383** 55
[20] Breuer M, Wessling S, Schmalzl J and Hansen U 2004 *Phys. Rev. E* **69** 026302
[21] Schmalzl J, Breuer M and Hansen U 2004 *Europhys. Lett.* **67** 390
[22] Alhers G and Xu X C 2001 *Phys. Rev. Lett.* **86** 3320
[23] van der Poel E P, Stevens R J A M and Lohse D 2013 *J. Fluid Mech.* **736** 177
[24] Roche P E, Castaing B, Chabaud B and Hébral B 2002 *Europhys. Lett.* **58** 693
[25] Li X M, He J D, Tian Y, Hao P and Huang S D 2021 *J. Fluid Mech.* **915** A60
[26] Lam S, Shang X D, Zhou S Q and Xia K Q 2002 *Phys. Rev. E* **65** 066306
[27] Lohse D and Grossmann S 2002 *Phys. Rev. E* **66** 016305
[28] Huang S D, Kaczorowski M, Ni R and Xia K Q 2013 *Phys. Rev. Lett.* **111** 104501
[29] Zhou W F and Chen J 2018 *Phys. Fluids* **30** 111705
[30] Zou H Y, Zhou W F, Chen X, Bao Y, Chen J and She Z S 2019 *Acta Mechanica Sinica* **35** 713
[31] Huang Y X and Zhou Q 2013 *J. Fluid Mech.* **737** R3
[32] Gao Z Y, Luo J H and Bao Y 2018 *Chin. Phys. B* **27** 104702
[33] Bao Y, Luo J H and Ye M X 2017 *J. Mech.* **34** 159
[34] Bao Y, He J C and Gao Z Y 2019 *Acta Phys. Sin.* **68** 16 (in Chinese)
[35] Zhang Y, Zhou Q and Sun C 2017 *J. Fluid Mech.* **814** 165
[36] Sugiyama K, Ni R, Stevens R J A M, Chan T S, Zhou S Q, Xi H D, Sun C, Grossmann S, Xia K Q and Lohse D 2010 *Phys. Rev. Lett.* **105** 034503
[37] Chandra M and Verma M K 2011 *Phys. Rev. E* **83** 067303
[38] Wang Q, Xia S N, Wang B F, Sun D J, Zhou Q and Wan Z H 2018 *J. Fluid Mech.* **849** 355
[39] Xu A, Chen X and Xi H D 2021 *J. Fluid Mech.* **910** A33
[40] Chen X, Huang S D, Xia K Q and Xi H D 2019 *J. Fluid Mech.* **877** R1
[41] Sugiyama K, Calzavarini E, Grossmann S and Lohse D 2009 *J. Fluid Mech.* **637** 105
[42] van der Poel E P, Stevens R J A M and Lohse D 2011 *Phys. Rev. E* **84** 045303
[43] van der Poel E P, Stevens R J A M, Sugiyama K and Lohse D 2012 *Phys. Fluids* **24** 085104